Temperature controlled tundra fire severity and frequency during the last millennium in the Yukon-Kuskokwim Delta, Alaska

Jarunetr Sae-Lim[1, †, *], James M Russell[1,2], Richard S Vachula[1,2], Robert M Holmes[3], Paul J Mann[3,4], John D Schade[3], Susan M Natali[3]

[1] Department of Earth, Environmental and Planetary Sciences, Box 1846, 324 Brook St., Providence RI 02912, USA

[2] Institute at Brown for Environment & Society, Brown University, Providence RI 02912, USA

[3] Woods Hole Research Center, 149 Woods Hole Road, Falmouth MA 02540

[4] Department of Geography, Northumbria University, Newcastle Upon Tyne, UK

[†] *Present address*: Department of Earth and Planetary Sciences, Washington University, 1 Brookings Drive, Campus box 1169, St. Louis MO 63130, USA

*Corresponding author: Jarunetr Sae-Lim, jsae-lim@wustl.edu, +1(401) 338-5788

Abstract

Wildfire is an important disturbance to Arctic tundra ecosystems. In the coming decades, tundra fire frequency, intensity and extent are projected to increase due to anthropogenic climate change. To more accurately predict the effects of climate change on tundra fire regimes, it is critical to have detailed knowledge of the natural frequency and extent of past wildfires and how they responded to past climate variability. We present analyses of fire frequency and temperature from a lake sediment core from the Yukon-Kuskokwim (YK) Delta. Our ca. one thousand macroscopic charcoal record shows more frequent but possibly less severe tundra fires during the first half of the last millennium, whereas less frequent, possibly more severe fires characterize the latter half . Our temperature reconstruction, based on distributional changes of branched glycerol dialkyl glycerol tetraethers (brGDGTs), shows slightly warmer conditions from ca. AD 1000 to 1500, and cooler conditions thereafter (ca. AD 1500 to 2000), suggesting that fire frequency increases when climate is relatively warmer in this region. When wildfires occur more frequently, fire severity may decrease due to limited biomass (fuel source) accumulating between fires. The data suggest that tundra ecosystems are highly sensitive to climate change, and that a warmer climate, which is predicted to develop in the near future, will result in more frequent tundra wildfires.

Keywords

Arctic, Alaska, paleofire, late Holocene, paleoclimate, glycerol dialkyl glycerol tetraethers (GDGTs), charcoal

Introduction

Arctic tundra, characterized by an extremely cold climate, a short growing season, a treeless landscape, and permafrost, is one of the most vulnerable ecosystems on Earth (ACIA, 2004). This biome also plays an important role as one of the largest carbon sinks on Earth, where about half of the Earth's soil organic carbon is stored in permafrost (Schuur et al., 2008). For the last several decades, Arctic air temperatures have increased at twice the global average rate (IPCC, 2013; McBean et al., 2005). This warming can affect many important processes in Arctic tundra ecosystems, including wildfire regimes (Higuera et al., 2011). Wildfires are one of the most critical disturbances in the Arctic tundra region as they contribute to permafrost thawing, vegetation changes, and carbon release (Jones et al., 2015; Loranty et al., 2016). Indeed, Arctic wildfires can abruptly perturb regional carbon cycling and release significant quantities of permafrost carbon to the atmosphere (Mack et al., 2011). This release may act as a positive feedback to a warming climate and promotes further release of stored carbon via permafrost thaw, thereby constituting a serious threat to global climate (Schuur et al., 2008; Qiu, 2009).

Arctic climates are predicted to warm in the future (IPCC, 2013; Boisvert and Stroeve, 2015; Miller et al., 2010). However, projecting changes in Arctic tundra wildfire regimes is difficult because of the many interrelated factors that control wildfires, including temperature, precipitation, soil moisture, and vegetation (Whitlock et al., 2010). Although a few studies have suggested that wildfires occur more frequently under a warmer and dryer climate in northern Alaska (Higuera et al., 2008; Hu et al., 2010; Daniau et al., 2010), records of Arctic fire are few, and records from different tundra locations and time periods often show contradictory results. For example, Chipman et al. (2015) and Vachula et al. (2018) observed more frequent wildfires in southwestern and northern Alaska, respectively during the last glacial period (36,000 yr BP to

12,000 yr BP) when temperatures were colder than today, in contrast to predictions of increased fire frequency as climate warms (Hu et al., 2015; Hu et al., 2010). Many fire records in the Arctic tundra also have coarse temporal resolution (e.g. Chipman et al., 2015; Higuera et al., 2011), and temperature records often are not derived from the same location as fire records. Thus, although existing fire records from the tundra have provided considerable insight into fire dynamics (Hu et al., 2015; Chipman et al., 2015; Higuera et al., 2011; Gavin et al., 2007; Vachula et al., 2018), we continue to lack knowledge of the relationships between tundra fires and temperature on decadal to centennial timescales, which could provide insight into tundra fire sensitivity to anthropogenic climate change. A high-resolution record of wildfires with a corresponding temperature record from the same study site could provide a significant advance in our understanding of Arctic fires and ecosystems.

In this study, we investigate how climate influences Arctic wildfires by generating a high-resolution, millennium-long record of fire and mean annual temperature using a lake sediment core from the Yukon-Kuskokwim (YK) Delta, Alaska. The fire record is based on macroscopic charcoal analyses, whereas our temperature reconstruction is based on distributional variations of branched glycerol dialkyl glycerol tetraethers (brGDGTs). We also use GIS analyses to compare the reconstructed fire record with historically documented fires to evaluate the sensitivity of the macroscopic charcoal record. Charcoal records provide insight into local tundra fires (i.e. fires occurring in a 10 km^2 to 100 km^2 region; Higuera et al., 2007). Similarly, brGDGTs record local temperature (Russell et al., 2018), though they may provide additional insight into larger-scale climate changes. These data allow us to determine the relationships between fires and temperature of the YK Delta and will contribute to more accurate projections of Arctic tundra fire regime under the changing climate.

Methods

Study Site

Lake Lin (unofficial name; 61.28721 °N, 163.26052 °W, 2.43 m a.s.l.) is situated in the YK Delta, Alaska (Figure 1). It has a surface area of ~0.3 ha and small inlet and outlet streams. In June 2017, the depth of the lake was ~1 m. The region is characterized by low-shrub tundra with discontinuous permafrost and abundant shallow thermokarst lakes. The local landscape has a thick organic soil (20-30 cm thick) with clusters of vegetation, and charred plants on the surface. Vegetation cover is composed of mosses, lichens, grasses (e.g. polar grass *Arctagrostis angustifolium*, tall cotton grass *Eriophorum angustifolium*), herbs and shrubs (e.g. tall firewood *Epilobium augustifolium* Labrador tea *Ledum palustre*, crowberry *Empetrum nigrum*, bog cranberry *Oxycoccus microcarpus*, salmonberry *Rubus chamarmorus*, and blueberry *Vaccinium uliginosum*). Lichen is the dominant vegetation type in the unburned area, whereas herbs are dominant vegetation type in the burned scars. Historical weather data (1926-2016) from the nearby Bethel Airport Station (PABE) indicate that the average annual temperature of the area is -1.02 ± 1.40°C, and average total annual precipitation is 441±123 mm. The average summer (June-August; JJA) temperature is 11.86 ± 0.99°C, and average total JJA precipitation is 188 ± 65 mm. Based on NCEP/NCAR Reanalysis (Kalnay et al., 1996), the AD 1948-2017 composite mean of surface wind in the YK Delta is ~1-1.25 m/s.

Sediment coring

A lake sediment core was collected from the deepest part of Lake Lin in July 2017 using a rod-operated piston corer with a polycarbonate tube (68 mm diameter). Special care was taken

to ensure recovery of the sediment-water interface. The core was sliced into contiguous, ~0.5 cm increments in the field, packed and shipped back to the laboratory at Brown University. Limited field equipment may have resulted in small uncertainties in the length of extruded intervals. Therefore, we determined the sediment mass per extruded interval to correct for variations in the thickness of each sample, assuming similar mass and density from interval to interval. To do so, 3 cm^3 subsamples were taken from every slice to determine wet weight, dry weight, and thereby bulk density and moisture content. The bulk density was used to calculate the sediment mass per interval, and the mass per interval was divided by the surface area of the piston corer to obtain the corrected thickness per interval.

The sediment chronology and age-depth model were constructed from accelerator mass spectrometry ^{14}C dating of terrestrial macrofossils (leaves, stems and twigs) from 4 depths spread along the core. Macrofossils were submitted to National Ocean Sciences Accelerator Mass Spectrometry (NOSAMS) at Woods Hole Oceanographic Institution for radiocarbon dating. All radiocarbon ages from NOSAMS were calibrated to AD years using the IntCal 13.14C dataset from CALIB 7.1 (Reimer et al., 2018). We assume that the core top represents modern time (AD 2017), and developed an age model using a polynomial regression in *Clam 2.2* software (Blaauw, 2010).

Macroscopic charcoal analysis

A 1 cm^3 subsample was taken from every core interval and placed in a centrifuge tube with 0.025 M sodium pyrophosphate and 2.5% sodium hypochlorite overnight (Chipman et al., 2015). The treated subsamples were washed with distilled water through a 250 μm sieve. This macrocharcoal fraction (>250 μm) was identified and counted under a microscope at 10x40

magnification (Chipman et al., 2015). The Charcoal Accumulation Rate (CHAR, charcoal particles cm^{-2} yr^{-1}) was calculated by multiplying the charcoal concentration (particles/cm^3) by the sediment accumulation rate (cm/yr).

The fire history was inferred based on the magnitude and temporal pattern of CHAR peaks. *CharAnalysis* 1.1 software was used to statistically interpret the local fire history based on defined thresholds to separate fire signals from noise (Higuera et al., 2007). For this study, the background was smoothed with a 200-yr running mean. A Gaussian mixing model was used to identify the mean and variance of the background distribution, and the 90th percentile of this distribution was used as the threshold. Any peaks that exceeded this threshold were identified as a fire episode. We chose the 90th percentile in order to contextualize past burning with reference to the 2015 fire, which registered as an episode using this threshold. *CharAnalysis* typically reports only the absolute dates of CHAR peaks. We rounded the *CHARAnalysis* derived fire years to the nearest ten, and the uncertainty of CHAR peaks was then derived from the average uncertainty of the age-depth model.

Fire frequency (fires/200 yr) and fire return interval (FRI; yr/fire) were calculated using our age model and the charcoal data. We divided the record into zones based on visual observations of fire return intervals and a student's t-test applied to evaluate whether changes in fire frequency differed significantly between visually-identified zones.

Geographic information system (GIS)-observed fire analysis

To evaluate the frequency and severity of the observed fires during the last ca. 80 years, we analyzed data from the Alaska Interagency Coordination Center using ArcGIS Pro software. The 1940-2015 Alaskan wildfire shape-files of area burned with fire years were downloaded and

spatial maps of wildfire locations in the YK Delta were created. The final maps were created in the NAD 1983 (2011) State Plane Alaska 2 FIPS 5002 coordinate system, and used the Transverse Mercator projection.

Glycerol dialkyl glycerol tetraether analysis

Temperature reconstruction was based on distributional variations of branched glycerol dialkyl glycerol tetraethers (brGDGTs). BrGDGTs are membrane-spanning lipids produced by bacteria. They are found nearly ubiquitously in lake and marine sediments, peats, and other deposits. Many studies have shown that the bacteria alter the structure of their brGDGTs to maintain membrane fluidity in response to changes in environmental temperature and chemistry (Russell et al., 2018; Schouten et al., 2013). Empirical studies have used these relationships to develop calibrations of the relative abundances of brGDGTs to mean annual air temperature and pH (Weijiers et al., 2007.; Peterse et al., 2009; De Jonge et al., 2014).

To analyze the brGDGTs, a 1 cm^3 subsample was taken from 20 homogenized lake sediment samples and freeze dried. The lipids were extracted with 9:1 dichloromethane:methanol (DCM:MeOH, v/v) using a Dionex™ accelerated solvent extraction (ASE 350) system. Extracts were separated into non-polar and polar fractions via flash chromatography using Al_2O_3 columns and 9:1 hexane:DCM and 1:1 DCM:MeOH as eluents. The polar fractions, captured in the 1:1 DCM:MeOH elution, were dried, reconstituted, and filtered, and then analyzed through high performance liquid chromatography/atmospheric pressure chemical ionization-mass spectrometry (HPLC/APCI-MS) using the analytical protocol of Hopmans et al. (2016) to separate 5- and 6-methyl brGDGT isomers. Analyses were performed using the selective ion monitoring (SIM) mode to track m/z 1302, 1300, 1298, 1296, 1292, 1050, 1048, 1046, 1036,

1034, 1032, 1022, 1020, 1018, and 744. brGDGTs were quantified by integration of the peak areas (Loomis et al., 2015; Russell et al., 2018).

Many studies have shown that under the same temperatures, the relative abundances of brGDGTs in soils and those in lake sediment differ (Buckles et al., 2014; Loomis et al., 2014). Therefore, both soil-specific calibrations and lake-specific calibrations exist to convert brGDGT distributions to temperature, depending on brGDGT source. As soil- and lacustrine calibrations can differ by nearly 10 ºC, misapplication of brGDGT calibrations will result in unrealistic reconstructed temperatures (Tierney and Russell, 2009; Loomis et al., 2014; Watson et al., 2018). In this study, we used soil-based calibrations from De Jonge et al. (2014) to reconstruct mean annual air temperatures (MAAT), as the temperatures inferred from core-top samples using this calibration most closely resemble the modern annual mean. Application of lacustrine calibrations results much colder values than expected, which is common given the different intercepts of lacustrine and soil-derived brGDGT calibrations (Loomis et al., 2014; Russell et al., 2018; Watson et al., 2018).

The mean annual air temperature was calculated from the fractional abundances of the brGDGT summed into 3 different indices based on calibrations from De Jonge et al. (2014):

1) Index 1 (MAT_{index1})

$$\text{Index 1} = {}^{10}\log\left[(\mathbf{I}a + \mathbf{I}b + \mathbf{I}c + \mathbf{II}a' + \mathbf{III}a')/(\mathbf{I}c + \mathbf{II}a + \mathbf{III}a + \mathbf{III}a')\right]$$

$$MAT_{index1} = 5.05 + 14.86*\text{Index 1}$$

2) Multiple linear regression-based mean air temperature (MAT_{mr})

$$MAT_{mr} = 7.17 + 17.1*[\mathbf{I}a] + 25.9*[\mathbf{I}b] + 34.4*[\mathbf{I}c] - 28.6*[\mathbf{II}a]$$

3) The degree of methylation of branched tetraethers (MBT) using 5-methyl isomers only ($MAAT_{MBT'5ME}$)

$$MBT'_{5ME} = (\mathbf{I}a + \mathbf{I}b + \mathbf{I}c)/(\mathbf{I}a + \mathbf{I}b + \mathbf{I}c + \mathbf{II}a + \mathbf{II}b + \mathbf{II}c + \mathbf{III}a)$$

$$MAAT_{MBT'5ME} = -8.57 + 31.45*MBT'_{5ME}$$

where **I**a, **I**b, etc. refer to the fractional abundance of the structures of brGDGTs.

Weather data collected at PABE (1926-2017) were used to estimate modern temperatures to evaluate the most suitable temperature index for the temperature reconstruction.

Results

Sediment core chronology

The 51.5 cm long core was composed of dark brown, organic-rich clays with thin beds of terrestrial macrofossils (small leaves and twigs) at 19.5 cm and 31.5 cm. Our age-depth model is based on two radiocarbon dates at 12.75 and 48.45 cm depth, and an assumption that the core top dates to the year of core recovery. Two other ^{14}C dates were excluded from the age-depth model because they were stratigraphically too old compared to other ages (540 BC at 25.15 cm) or too young (>AD 1950, at 38.92 cm) compared to overlying ages (Table 1). The anomalously old date likely resulted from reworking of macrofossils from erosion of old soil/permafrost; such reworked terrestrial macrofossils are common in Arctic lake sediments (Oswald et al., 2005). The cause of the abnormally young date is more difficult to explain, but likely resulted from sample contamination or movement of the macrofossil during core acquisition or extrusion. Including this age would require rejection of all other ^{14}C ages in the core are would imply sedimentation rate on the order of ~1 cm/yr, much higher than values typically observed in the Arctic (Hermanson, 1990).

We assumed that the core top represents the year of core acquisition, AD 2017. We are confident that we recovered the sediment water interface, as we observed an intact sediment-

water interface in the field, and we observe peak in charcoal concentration in the uppermost sample that likely corresponds to a fire in AD 2015. Although it is possible that the sediment at the core top is truly not modern (i.e. that our core site has not received recent sediments), Lake Lin is small and shallow, and we carefully selected the core location to provide a continuous, representative and undisturbed sequence. We cored at the deepest and flat part of the lake to avoid shoreline erosion since deeper and flatter areas tends to be less prone to mixing processes in shallow lakes (Smol, 2008). We also avoided close to the inlet and outlet in order to minimize a possibility of mixing due to water flows.

The age-depth model indicates that the core extends to about AD 1000 (AD 820 - 1160 at 95% confidence interval; Figure 2). We chose a regression (order = 1) for our age-depth model because other model types resulted in abrupt changes in sedimentation rates due to artefacts of the age-depth models or age reversals. The model estimated sedimentation rates to be 0.05 cm/yr from AD 1000 to the core top.

Fire history

CHARs and charcoal background rates are variable throughout the core (Figure 3a). *CharAnalysis* identified seven charcoal peaks as fire episodes with ages (at the top of each of the samples) of AD 1100, 1210, 1300, 1420, 1680, 1860, and 2017, with an average age uncertainty of ±30 years. One additional charcoal peak at AD 1040 was identified as a possible fire episode. We infer the charcoal peak in the topmost sample to be derived from the AD 2015 fire, which is the only fire to observed have occurred within 3 km of the lake. Four peaks show equal or greater peak magnitude to the most recent, AD 2015 fire.

Fire frequency in our record remained constant at 1 fire/100 yr from ~AD 1000 to 1300. After AD 1300, the frequencies decline to a minimum 0.26 fires/100 yr by AD 1550 (Figure 3b). Fire frequencies fluctuate after AD 1550 but never reach the pre-1300 frequency of 1 fires/100 yr (Figure 3b). Based on these estimates of FRIs, we divide the fire record into 2 intervals: Zone 1, from AD ~1000-1420, and Zone 2, from AD ~1420-2017. The FRI mean and standard deviation for Zone 1 are 94 ± 27 yr/fire, whereas those of Zone 2 are 199 ± 44 yr/fire. A student's t-test of the mean FRI between these two zones indicates the two means are significantly different (p-value < 0.05). Although Zone 2 shows less frequent fire episodes, the fire episodes in Zone 2 generally have higher CHAR values than fire episodes in Zone 1. Though the differences are not statistically significant, the higher CHAR values may suggest larger and/or more intense fires.

The YK Delta experienced a major fire in AD 2015. Three other recent wildfires were recorded within a 10-km radius of Lake Lin, namely fires in AD 1972, 1988, and 2002. The boundaries of some of these fire events overlapped, indicating repeated burning of some areas. Lake Lin is located inside the AD 2015 burn, whereas the older burns are at least 4 km away from Lake Lin, and the sizes of these old burns are 10-70 times smaller than the AD 2015 burn (Figure 4). The uppermost sediment sample (AD 2015-2017) has a charcoal peak corresponding to the AD 2015 fire event. Other burns during historical time were not recorded as fire events in the CHAR record.

Mean annual temperature history

Mean annual temperatures estimated from the three brGDGT indices, $MAAT_{index1}$, $MAAT_{MR}$, and MBT'_{5ME}, show similar trends over the last millennium (Figure 5). The $MAAT_{MBT'5ME}$ shows the highest overall temperature values, whereas the MAT_{mr} shows the

lowest overall temperature values. The temperatures inferred from the $MAAT_{MBT'5ME}$ in the uppermost sediments (-0.61 °C) are closest to the average annual temperature at AD 2015 at PABE (1.16 °C), so we use this index to represent the temperature history of our site.

The $MAAT_{MBT'5ME}$ record shows only modest variability, with a slight overall cooling trend over time (Figure 3c). We examined the relationship between temperatures in Zones 1 and 2 defined by our fire record and found that the means of these two temperature zones were significantly different in a student's t-test ($p < 0.001$), though it must be noted that the errors of the de Jonge et al. (2014) calibration greatly exceed the average temperature difference between Zones 1 and 2. The mean of Zone 1 is 0.47 °C warmer than the mean from zone 2. This 0.47 °C cooling is well within the brGDGT calibration uncertainty; however, the overall trend is generally compatible with other reconstructions from Arctic Alaska, as discussed below.

Reconstructed mean annual temperatures show a weak positive relationship with the fire record (Figure 3). During the warmer period (Zone 1), the FRI is shorter and fire episodes have lower CHAR values. During the cooler period (Zone 2), the FRI is longer and fire episodes show greater CHAR values.

Discussion

The fire history of the Yukon-Kuskokwim Delta, Alaska

Our charcoal record documents 8 major fire episodes over the last millennium. Comparing our record to macroscopic charcoal records from other sites in Alaska, we found that the Lake Lin region experienced more fire episodes during the last millennium and shorter overall mean FRI than other records (Figure 6; Table 2). Some lakes, particularly those on the North Slope, record one or fewer fire episodes during the last 1,000 years (Hu et al., 2015;

Chipman et al., 2015), whereas Lake Lin recorded 8 major fire episodes, four of which have a CHAR value equal to or greater than the most severe fire in the historical record, the AD 2015 fire event. Although some charcoal records from the Noatak watershed exhibit similar numbers of fire episodes as Lake Lin (Higuera et al., 2011), the Noatak watershed is located within a transition zone from boreal forest to tundra, so the fire regime in this region is different from typical tundra ecosystems as wildfires in boreal forest are more frequent and more intense than those in tundra (Stocks et al., 2001). Besides geographical differences, the resolution of the charcoal records might contribute to differences in numbers of detected fire episodes. Records with a higher resolution will have more ability to detect frequent fires, resulting higher numbers of fire events. However, this does not fully explain the variability among the records. For instance, the record from Keche Lake shows only one fire episode over the last 1,000 years in spite of a similar resolution to that of Lake Lin (18 years/sample; Hu et al., 2015)

Charcoal records from within the YK Delta are also variable. Tungak Lake, located approximately 52.8 km to the west of Lake Lin, is about 400 times larger and 15 times deeper than Lake Lin (Chipman et al., 2015). The charcoal record from this lake shows no sign of fire over the last 6,500 years, and the mean FRI of this lake is very long (5905 year/fire; range = 1157-9968 years/fire; interpolation interval = 89 years/sample; method: macroscopic charcoal analysis, mesh size = 125 μm; Chipman et al., 2015). Many factors could affect the amount of charcoal inputs to a lake including the number of actual fires around the lake, fire temperature, distance between fire and the lake, lake size and watershed size, and particle density, shape and size (Higuera et al., 2007; Peters and Higuera, 2007; Vachula and Richter, 2017). Tungak Lake and Lake Lin likely experienced a similar fire history as they are situated in the same ecosystem and climate. Though there are small hills surrounding Tungak, Lin and Tungak lie in the same

watershed (Reid and Fehringer, 2018) and share similar vegetation and climate (precipitation and temperature). Further, the majority of fires are located to the east of Tungak and Lin, and winds are predominantly easterlies, so wind-driven differences in charcoal transport to the lakes are unlikely to have caused this disconnect. Therefore, the size of the lake and the dispersal distance of charcoal particles likely contribute to the differences in CHAR rates and fire episodes. Atmospheric deposition and rivers can introduce charcoal particles to the lake (Whitlock et al., 2002), and charcoal particles likely sink very close to the inlet, shoreline, or point where they fell from the air onto the lake. Coring locations in the center of a large lake, such as Tungak, may therefore detect fewer fires than in a small lake, such as Lake Lin (Mustaphi et al., 2015).

That said, our GIS analysis shows that there is no observed fire within a 20-km radius from Tungak Lake (Figure 7). In contrast, Lake Lin is located within the burned area of the AD 2015 fire event, and approximately 5 km away from three other small known fires. Although these smaller events did not result in CHAR peaks crossing our threshold for background variability, a CHAR peak at ~AD 1980 might correlate with the AD 1972 fire event, which is above the natural background line but lower than our threshold. Thus, the fire record from Lake Lin macrocharcoal (>250 μm) can record tundra fires at the local scale (<5 km from the lake). The frequency of fires recorded in Lake Lin relative to other regional sites suggests Lake Lin is quite sensitive to local fires, and that the region around the lake has burned frequently during the last ~1,000 years.

The temperature of the last millennium in the Yukon-Kuskokwim Delta, Alaska

To our knowledge, the Lake Lin brGDGT analysis represents the first temperature record spanning the last millennium from the YK Delta, Alaska. A lack of tree-ring records from this

region, our age model uncertainty, and the coarse resolution of other regional paleolimnological temperature reconstructions (e.g. Kurek et al., 2008) prohibit tests of correlation of our record to other regional records. Nevertheless, comparisons of our temperature record to global and regional temperature syntheses, including a pan-Arctic temperature synthesis and an Alaskan temperature synthesis (Kaufman et al., 2009; Bird et al., 2008; McKay and Kaufman, 2008; D'Arrigo et al., 2007; Loso et al., 2006), indicate similarities and differences.

Overall, the mean annual temperature reconstruction from Lake Lin shows a slight cooling over the last millennium. A similar cooling trend is observed in other records including the Arctic temperature composite record and Alaska temperature composite record (Figure 8; Kaufman et al., 2009; Bird et al., 2008; McKay and Kaufman, 2008; D'Arrigo et al., 2007; Loso et al., 2006). Although the Lake Lin record has a coarser resolution than these records, and despite the uncertainty in our age model, we can still observe some correlations of centennial-scale temperature variability among these records, such as temperature minima around AD 1200-1300, AD 1500-1550, and AD 1700. Further, these temperature minima generally correspond to glacier fluctuation in the Ahklun Mountains that suggest Little Ice Age cooling between AD 1300 and 1750 (Levy et al., 2004).

In contrast, the 20th century warming observed in the Arctic and Alaskan temperature composites is not apparent in the Lake Lin record, which shows a minor cooling (~ -0.5°C). This cooling is within the typical sample-to-sample variability of our brGDGT data, but it is also possible that the YK Delta has been less sensitive to anthropogenic warming over the last century than other regions in the Arctic, and might respond to the warming more slowly than other regions. Indeed, some observational and proxy records of temperature in Alaska also show a cooling trend during the last century, similar to that of Lake Lin (Southern Alaska: D'Arrigo et

al., 2007; and Northern Alaska: Husain, 2017). Analysis of weather data from the closest station to Lake Lin, the PABE weather station, indicates that mean annual temperatures from AD 1926 to 2016 were highly variable (range = -4.04-2.62°C), but do not show any significant warming or cooling trend. Alaska has been divided into 32 ecoregions based on climate and vegetation cover, and each ecoregion has its own unique climate and ecological characteristics (Nowacki et al., 2001). Therefore, we might not expect the same past climate pattern in the YK Delta as for other Alaskan ecoregions.

Relationships between fire and temperature in tundra environments

Although the chronology for our core creates challenges in comparing to other regional temperature records, we can evaluate the correlation between CHAR and temperature as these results were derived from the same core. Our CHAR record shows that the fire frequency of the YK Delta decreased over the last millennium. From AD 1000-1420, fires were more frequent but less intense, whereas from AD 1420-2017, fires became less frequent but more intense. The timing of this shift, at AD 1420 ± 20 corresponds to the brGDGT-inferred trend toward colder conditions in this region. Together, these data suggest that tundra wildfires occur less frequently when the climate is colder, and more frequently when the climate is warmer. This fire-climate relationship is supported by previous work in the Alaskan tundra (Hu et al., 2015; Young et al., 2017), which shows that wildfires occur more frequently in a warmer climate.

There are many processes by which a warming climate can increase wildfires in the Arctic. Lightning is the primary ignition source for tundra fires (Wein, 1976; Ververbeke et al., 2017), and the frequency of lightning strikes depends strongly on air temperature. Lightning strikes occur more frequently when the air temperature is higher because the air becomes more

convective (Del Genio et al., 2007; Romps et al., 2014; Wendel, 2014; Magi, 2014). Indeed, a few climate modeling studies have predicted an increase in total burned area in high latitudes as a result of expected higher numbers of lightning strikes resulting from climate warming (Ververbeke et al., 2017; Romps et al., 2014). Moreover, higher air temperature can contribute to a surface moisture deficit through evaporation, which leads to increased fire frequency. This moisture deficit results in a more flammable and fire-prone land surface, and therefore, more wildfires (Hu et al., 2010; Higuera et al., 2008). Warmer temperatures also promote vegetation growth that will become the fuel source (Tape et al., 2006; Bhatt et al., 2010). Though our data cannot directly offer insight into potential relationship between fire and precipitation in this region, this is an important consideration. Previous work in the YK Delta suggests that fire was promoted by arid conditions during the last glacial, despite cooler temperatures (Chipman et al., 2015). In contrast, data from a site in northern Alaska suggest cool and dry conditions alone cannot promote burning without temperature changes, which influence ignition (Vachula et al, 2019). These cases, in conjunction with our data, suggest that temperature, aridity, and ignition frequency have a complex relationship warranting further research.

Although fire frequency increased in the warmer conditions that existed during the first part of the last millennium, our data tentatively suggest higher CHAR magnitude during the colder conditions of the latter half of the last millennium. Typically, CHAR peak magnitude depends on fire severity, distance from the lake to the wildfires, and connectivity of fuel on the land, which can control fire extent (Power et al., 2008; Whitlock et al., 2010; Flannigan et al., 2009). The areal extent most likely depends on the availability of biomass and surface moisture budgets at the time a wildfire event occurs, which is controlled by climate (Higuera et al., 2008; Wein, 1976). A warmer climate often promotes tundra biomass growth and shrub expansion,

which can make fires more severe (Young et al, 2017; Whitlock et al., 2010). Higher air temperature can induce a surface moisture deficit, which can facilitate a wider area burned since fires tend to go further on a dry landscape than on a wet one (Flannigan et al., 2009; Liu et al., 2010). However, a warmer climate also shortens the FRI due to higher chances of ignition. More frequent fires will remove pre-existing biomass, inhibiting biomass accumulation. On the other hand, a cooler climate limits wildfires, which allows tundra biomass to accumulate, resulting in a more severe wildfire. Although these relationships have been previously documented in the Alaskan tundra, our study is the first to indicate that fire frequency and severity may be sensitive to modest temperature changes of the last millennium, highlighting the sensitivity of tundra ecosystems.

Conclusion

We reconstructed wildfire and climate history of the YK Delta, Alaska over the last millennium using multiproxy analyses of lake sediments. Our results show that wildfires occurred less frequently but possibly with increased severity over the past millennium as mean annual temperature became colder. Future climate is projected to change in the opposite direction—warmer climate as the result of current anthropogenic warming (IPCC,2013). This suggests that tundra wildfires could occur more frequently in the future. Furthermore, the fate of permafrost is directly tied to wildfires, with faster thaw as wildfires occur more frequently, and this positive feedback between permafrost, climate and wildfire could amplify the degree of global warming.

References

ACIA (2004) *Impacts of a warming arctic: Arctic climate impact assessment. ACIA overview report*. Cambridge University Press.

Bhatt US, Walker DA, Raynolds MK et al. (2010) Circumpolar arctic tundra vegetation change is linked to sea ice decline. *Earth Interactions,*14(8): 1-20.

Bird BW, Abbott MB, Finney BP et al. (2008) A 2000 year varve-based climate record from the central Brooks Range, Alaska. *Journal of Paleolimnology*,41(1): 25-41.

Blaauw M (2010) Methods and code for 'classical' age-modelling of radiocarbon sequences. *Quaternary Geochronology,5*(5): 512-518.

Boisvert LN andStroeve JC (2015) The Arctic is becoming warmer and wetter as revealed by the Atmospheric Infrared Sounder. *Geophysical Research Letters*,42(11): 4439-4446.

Buckles LK, Weijers JWH, Verschuren D, et al. (2014) Sources of core and intact branched tetraether membrane lipids in the lacustrine environment: anatomy of Lake Challa and its catchment, equatorial East Africa. *Geochimica et Cosmochimica Acta*,140: 106-126.

Chipman ML, Hudspith V, Higuera PE et al. (2015) Spatiotemporal patterns of tundra fires: Late-Quaternary charcoal records from Alaska. *Biogeosciences,*12(13): 4017-4027.

Chipman ML, Clarke GH, Clegg BF et al. (2009) A 2000 year record of climatic change at Ongoke Lake, southwest Alaska. *Journal of Paleolimnology,*41(1): 57-75.

Chipman ML, Clegg BF and Hu FS (2012) Variation in the moisture regime of northeastern interior Alaska and possible linkages to the Aleutian Low: Inferences from a late-Holocene δ18O record. *Journal of Paleolimnology,*48(1): 69-81.

Clegg BF and Hu FS (2010) An oxygen-isotope record of Holocene climate change in the south-central Brooks Range, Alaska. *Quaternary Science Reviews,*29(7-8): 928-939.

Crowley TJ (2000) Causes of climate change over the past 1000 years. *Science,*289(5477): 270-277.

Daniau A, Harrison S, and Bartlein P. (2010) Fire regimes during the Last Glacial. *Quaternary Science Reviews,*29(21-22): 2918-2930.

D'Arrigo R, Wilson R, Liepert B, et al. (2008) On the 'Divergence Problem' in northern forests: A review of the tree-ring evidence and possible causes. *Global and Planetary Change,*60(3-4), 289-305.

De Jonge C, Hopmans EC, Zell CI, et al. (2014) Occurrence and abundance of 6-methyl branched glycerol dialkyl glycerol tetraethers in soils: Implications for palaeoclimate reconstruction. *Geochimica Et Cosmochimica Acta,*141: 97-112.

Del Genio AD, Yao MS and Jonas J (2007) Will moist convection be stronger in a warmer climate? *Geophysical Research Letters*,34: L16703.

Fire History[Geographic information system shapefiles]. Wainwright: Alaska Interagency Coordination Center.

Flannigan MD, Krawchuk MA, de Groot WJ, et al. Implications of changing climate for global wildland fire. *International Journal of Wildland Fire*, 18: 483-507.

Gavin DG, Hallett DJ, Hu FS, et al. (2007) Forest fire and climate in western North America: insights from sediment charcoal records. *Frontiers in Ecology and the Environment,*5(9): 499-506.

Hale ME Jr (1959) Studies on lichen growth rate and succession. *Bulletin of the Torrey Botanical Club,*86(2): 126-129.

Hermanson MH (1990) ^{210}Pb and ^{137}Cs chronology of sediments from small, shallow Arctic lakes. *Geochimica et Cosmochimica Acta,54*(5): 1443-1451.

Higuera P, Peters M, Brubaker L, et al. (2007) Understanding the origin and analysis of sediment-charcoal records with a simulation model. *Quaternary Science Reviews,*26(13-14): 1790-1809.

Higuera PE, Brubaker LB, Anderson PM, et al. (2008) Frequent fires in ancient shrub tundra: implications of paleorecords for Arctic environmental change. *PLoS ONE,*3(3): e0001744

Higuera PE, Chipman ML, Barnes JL, et al. (2011) Variability of tundra fire regimes in Arctic Alaska: Millennial-scale patterns and ecological implications. *Ecological Applications,*21(8): 3211-3226.

Hopmans EC, Schouten S, and Sinninghe Damsté JS (2016) The effect of improved chromatography on GDGT-based palaeoproxies. *Organic Geochemistry*,93: 1-6

Hu FS, Ito E, Brown TA, et al. (2001) Pronounced climatic variations in Alaska during the last two millennia. *Proceedings of the National Academy of Sciences,*98(19): 10552-10556.

Hu FS, Higuera PE, Walsh JE, et al. (2010) Tundra burning in Alaska: Linkages to climatic change and sea ice retreat. *Journal of Geophysical Research,*115(G04002).

Hu FS, Higuera PE, Duffy P, et al. (2015) Arctic tundra fires: Natural variability and responses to climate change. *Frontiers in Ecology and the Environment*,13(7): 369-377.

Husain F (2017) *A Multiproxy Holocene Temperature Reconstruction from Northern Alaska.* Undergraduate thesis. Brown University, USA.

IPCC (2013) *Climate Change 2013: The Physical Science Basis. Contribution to the Fifth Assessment Report of the Intergovernmental Panel on Climate Change.* Cambridge University Press.

Jones BM, Grosse G, Arp CD, et al. (2015) Recent Arctic tundra fire initiates widespread thermokarst development. *Scientific Reports,*5(15865): 1-13.

Kalnay E, Kanamitsu M, Kistler R, et al. (1996) The NCEP/NCAR Reanalysis 40-year Project. Bull. *American Meteorological Society,*77: 437-471.

Kaufman DS, Schneider DP, Mckay NP, et al. (2009) Recent warming reverses long-term Arctic cooling. *Science,*325(5945): 1236-1239.

Kurek J, Cwynar LC, Ager TA, et al. (2009) Late Quaternary paleoclimate of western Alaska inferred from fossil chironomids and its relation to vegetation histories. *Quaternary Science Reviews,*28(9-10): 799-811.

Kylander ME, Ampel L, Wohlfarth B, et al. (2011) High-resolution X-ray fluorescence core scanning analysis of Les Echets (France) sedimentary sequence: New insights from chemical proxies. *Journal of Quaternary Science,*26(1): 109-117.

Levy LB, Kaufman DS and Werner A (2004) Holocene glacier fluctuations, Waskey Lake, northern Ahklun Mountains, southwestern Alaska. *Holocene,14*(2): 185-193.

Loomis SE, Russell JM, Ladd B, et al. (2012) Calibration and application of the branched GDGT temperature proxy on East African lake sediments. *Earth and Planetary Science Letters,*357-358: 277-288.

Loomis SE, Russell JM, Heureux AM, et al. (2014) Seasonal variability of branched glycerol dialkyl glycerol tetraethers (brGDGTs) in a temperate lake system. *Geochimica et Cosmochimica Acta,*144(1): 173-187.

Loranty MM, Lieberman-Cribbin W, Berner LT, et al. (2016) Spatial variation in vegetation productivity trends, fire disturbance, and soil carbon across arctic-boreal permafrost ecosystems. *Environmental Research Letters*,11(9): 095008.

Loso MG, Anderson RS, Anderson SP, et al. (2006) A 1500-year record of temperature and glacial response inferred from varved Iceberg Lake, southcentral Alaska. *Quaternary Research,*66(01): 12-24.

Liu Y, Stanturf J, and Goodrick S (2010) Trends in global wildfire potential in a changing climate. *Forest Ecology and Management*, 259: 685-697.

Mann ME, Zhang Z, Hughes MK, et al. (2008) Proxy-based reconstructions of hemispheric and global surface temperature variations over the past two millennia. *Proceedings of the National Academy of Sciences,*105(36): 13252-13257.

Mack MC, Bret-Harte MS, Hollingsworth TN, et al. (2011) Carbon loss from an unprecedented Arctic tundra wildfire. *Nature,*475(7357): 489-492.

Magi BI (2014) Globl Lightning Parameterization from CMIP5 Cliamte Model Output. *Journal of Atmospheric and Oceanic Technology*,32(3): 434-452.

McBean G, Alekseev G, Chen D, et al. (2005) Arctic climate: past and present. In *Arctic Climate Impact Assessment*. New York, NY: Cambridge University Press.

Mckay NP and Kaufman DS (2008) Holocene climate and glacier variability at Hallet and Greyling Lakes, Chugach Mountains, south-central Alaska. *Journal of Paleolimnology,*41(1): 143-159.

Miller GH, Alley RB, Brigham-Grette J (2010) Arctic amplification: can the past constrain the future? *Quaternary Science Reviews*,29(15-16): 17779-1790.

Morellón M, Valero-Garcés B, Vegas-Vilarrúbia T, et al. (2009) Lateglacial and Holocene palaeohydrology in the western Mediterranean region: The Lake Estanya record (NE Spain). *Quaternary Science Reviews,*28(25-26): 2582-2599.

Mustaphi CJC, Davis EL, Perreault JT, et al. (2015) Spatial variability of recent macroscopic charcoal deposition in a small montane lake and implications for reconstruction of watershed-scale fire regimes. *Paleolimnology*,54: 71-86.

Nowacki G, Spencer P, Fleming M, et al. (2001) Ecoregions of Alaska. Open file report 02-297. U.S. Geological Survey.

Oswald WW, Anderson PM, Brown TA, et al. (2005) Effects of sample mass and macrofossil type on radiocarbon dating of arctic and boreal lake sediments. *Holocene, 15*: 758-767.

Peters ME and Higuera PE (2007) Quantifying the source area of macroscopic charcoal with a particle dispersal model. *Quaternary Research,*67(02): 304-310.

Peterse F, Van Der Meer MT, Schouten S, et al. (2009) Assessment of soil *n*-alkane δ*D*and branched tetraether membrane lipid distributions as tools for paleoelevation reconstruction. *Biogeosciences Discussions,*6(5): 8609-8631.

Power MJ, Marlon J, Ortiz N, et al. (2008) Changes in fire regimes since the Last Glacial Maximum: an assessment based on a global synthesis and analysis of charcoal data. *Climate* Dynamics,30 (7-8): 887-907.

Qiu J (2009) Arctic ecology: Tundra's burning. *Nature*,461(7260): 34-36.

Reid FA and Fehringer D (2018) Yukon-Kuskokwim Delta: Yukon River Basin, Alaska (USA). In: Finlayson C, Milton G, Prentice R and Davison N (eds) *The Wetland Book.* Dordrecht: Springer.

Romps DM, Seeley JT, Vollaro D, et al. (2014) Projected increase in lightning strikes in the United States due to global warming. *Science*,346(6211): 851-854.

Russell JM, Hopmans EC, Loomis SE, et al. (2018) Distributions of 5- and 6-methyl branched glycerol dialkyl glycerol tetraethers (brGDGTs) in East African lake sediment: Effects of

temperature, pH, and new lacustrine paleotemperature calibrations. *Organic Geochemistry,*117: 56-69.

Schouten S, Hopmans EC, Sinninghe JS, et al. (2013) The organic geochemistry of glyceral tetraether lipids: A review. *Organic Geochemistry*,54: 19-26.

Schuur EA, Bockheim J, Canadell JG, et al. (2008) Vulnerability of permafrost carbon to climate change: implications for the global carbon cycle. *BioScience,*58(8): 701-714.

Smol JP (2008) *Pollution of lakes and rivers: a paleoenvironmental perspective.* Oxford: Blackwell Publications.

Stocks BJ, Wotton BM, Flannigan MD, et al. (2001) Boreal Forest Fire Regimes And Climate Change. In: Beniston M, Verstraete MM (eds) *Remote Sensing and Climate Modeling: Synergies and Limitations. Advances in Global Change Research*, 7. Springer: Dordrecht, pp 233-246.

Stuiver M, Reimer PJ and Reimer RW (2018) CALIB 7.1. Available at http://calib.org (accessed 7 April 2018).

Tape K, Sturm M and Racine C (2006) The evidence for shrub expansion in Northern Alaska and the Pan-Arctic. *Global Change Biology,*12(4): 686-702.

Tierney JE and Russell JM (2009) Distributions of branched CDCTs in a tropical lake system: implications for lacustrine application of the MBT/CBT paleoproxy. *Organic Geochemistry*,40: 1032-1036.

Vachula RS and Richter N (2017) Informing sedimentary charcoal-based fire reconstructions with a kinematic transport model. *The Holocene,*28(1): 173-178.

Vachula RS, Russell JM, Huang,Y, et al. (2018) Assessing the spatial fidelity of sedimentary charcoal size fractions as fire history proxies ith a high-resolution sediment record and historical data. *Palaeogeographic, Palaeoclimatology, Palaeoecology,508*: 166-175.

Veraverbeke S, Roger BM, Goulden ML, et al. (2017) Lightning as a major driver of recent large fire years in North American boreal forests. *Nature Climate Change,*7: 529-537.

Watson BI, Williams JW, Russell JM, et al. (2018) Temperature variations in the southern Great Lakes during the last deglaciation: Comparison between pollen and GDGT proxies. *Quaternary Science Reviews*,182: 78-92.

Weijers JW, Schefuss E, Schouten S, et al. (2007) Coupled thermal and hydrological evolution of tropical Africa over the last deglaciation. *Science,*315(5819): 1701-1704.

Wein R (1976) Frequency and Characteristics of Arctic Tundra Fires. *ARCTIC*, 29(4), pp.213-222.

Wendel J (2014). Lightning strikes predicted to increase as climate warms. *Eox, Transactions American Geophysical Uniion,*95(47): 431.

Western Regional Climate Center (2018). Bethel Historical Climate Records. Available at: www.wrcc.dri.edu/summary/Climsmak.html (accessed 1 February 2018).

Whitlock C and Larsen C (2002) Charcoal as a fire proxy. *Tracking Environmental Change Using Lake Sediments Developments in Paleoenvironmental Research*,3: 75-97.

Whitlock C, Higuera PE, McWethy, DB, et al. (2010) Paleoecological Perspectives on Fire Ecology: Revisiting the Fire-Regime Concept. *The Open Ecology Journal*,3(2): 6-23.

Young AM, Higuera PE, Duffy PA, et al. (2017) Climatic thresholds shape northern high-latitude fire regimes and imply vulnerability to future climate change. *Ecography,*40(5): 606-617.

Acknowledgements

We thank S. Ludwig for field assistance, and L. Messier for lab assistance. Funding for this research was provided by the Polaris Project Fellowship sponsored by Woods Hole Research Center (NSF-1624927) and a VOSS Undergraduate Research Fellowship in Environmental Science and Communication sponsored by the Institute at Brown for Environment and Society to J. Sae-Lim.

Table 1. Radiocarbon ages and calculated calendar ages

Sample depth (cm)	Materials	NOSAMS sample code	^{14}C AMS age (yr BP)	Calibrated calendar age (yr)
12.75	Twigs	148150	335 ± 15	AD 1579±22
25.15	Leaves	148149	2490 ± 20	618±78 BC
38.92	Twigs	148148	>Modern	AD >1950
48.45	Small parts of plants	148147	915 ±20	AD 1101±63

Table 2. Site and charcoal record comparison

Characteristic	Lin	Tungak	Perch	Upper Capsule	Keche	Raven	Uchugrak	Poktovik	Little Isac
Site									
Ecoregion	YK Delta	YK Delta	North Slope	North Slope	Brook Range	Noatak Watershed[1]	Noatak Watershed[1]	Noatak Watershed[1]	Noatak Watershed[1]
Land cover class	Low-shrub tundra	Low-shrub tundra	Dwarf-shrub tundra	Dwarf-shrub tundra	Boreal Transition	Tussock-shrub tundra with white spruce	Tussock-shrub tundra	Tussock-shrub tundra	Tussock-shrub tundra
Mean JJA temperature (°C)[2]	11.86±0.99	12.3±0.1	10.9±0.04	10.0±0.1	10.8±0.5	12.27±0.07	12.10±0.15	11.93±0.10	11.87±0.32
Total JJA precipitation (mm)[2]	180±60	169±2	101±5	187±7	142±14	149±1	153±2	152±2	146±4
Surface area (m^2)	2955.6	1170000	140000	11000	802000	57000	37000	63000	29000
Coring water depth (m)	1	14.8	12.6	5.7	14.5	4.9	9.2	13.4	5.4
Record									
Sediment accumulation rate (cm/yr)	0.0496	0.030±0.039	0.045±0.080	0.031±0.011	0.030±0.027	0.0490±0.3591	0.0479±0.0960	0.0475±0.1912	0.0206±0.0367
Average (range) charcoal concentration (particle · cm^{-3})	6.72 (2.1-27)	0.19 (0-6.25)	0.56 (0-28.5)	0.14 (0-2.75)	0.29 (0-34.0)	1.89 (0-13.56)	1.49 (0-24.4)	0.73 (0-13.56)	2.54 (0-23.49)
Interpolation interval (yr/sample)	13	89	43	65	18	15	15	15	15
Range of FRIs (yr)	>65 to 260	1157 to >9968	2924–6536	>5590 to >6500	144–3906	30-285	45-345	45-525	60-840
Mean FRI (yr)	141	5904	4730	6045	1648	151	135	227	309
Most recent FRI (yr)	156	>7031	6536	>6500	>882	105	75	120	840
Number of peaks identified as fires during the last 1,000 years	8*	1*	1	0	1*	6	8	9	3

[1] Transition zone from boreal forest to tundra

[2] June-August average temperature and precipitation from PABE spanning from 1926-2016 (Lin), and PRISM-derived data spanning from 1971-2000 (Tungak, Perch, Upper Capsule, Keche; Chipman et al., 2015, and Raven, Uchugak, Poltovik, Little Isac; Higuera et al. 2011)

* Include peaks that did not pass the screen test

Figure captions

Figure 1. GIS maps of the study region, and locations of published Alaskan records. Map of Alaska with ecoregions represented in different colors (Nowacki et al., 2001). Green, dark gray, medium gray and light gray patches show the YK Delta, tundra, temperate continental and temperate coastal, respectively. The black circles denote major Alaskan cities. The black star represents Lake Lin, our study site. The red circles show locations of published charcoal records (Chipman et al., 2015; Higuera et al., 2011). The blue circles show locations of Alaskan temperature reconstructions (published: Kaufman et al., 2009; Bird et al., 2008; Mckay and Kaufman, 2008; Loso et al., 2006; Kurek et al., 2008; unpublished: Husain, 2017).

Figure 2: Age-depth model for Lake Lin with AMS ^{14}C dates (blue). The black line shows the mean age-depth plot and the gray shading represents uncertainty of the age-depth plot at 95% confidence ranges. The light blue mark at the top right corner represents the coring year (AD 2017). The dark blue marks are radiocarbon dates. The red mark represents the excluded abnormally young radiocarbon date. The abnormally old radiocarbon date is not shown.

Figure 3: Fire and climate history of the YK Delta, Alaska. a) CHAR variability over the last millennium. Black bars represent CHAR throughout the core. The gray line represents CHAR background, while the red line shows the 90% threshold or cutoff. Peaks that passed the red line were counted as fire episodes as indicated by red plus symbol. A gray dot represents a major fire episode that failed *CharAnalysis* test. b) Fire frequency (number of fires over 200 years). c) The reconstructed temperature of the region, based on MBT'$_{5ME}$ index. This composited plot was

divided into two zones based on FRIs. Zone 1 (gray shading) represents the time from AD 1000-1420, and Zone 2 (white shading) represents the time between AD 1420 to present.

Figure 4: Map of Lake Lin and known wildfires within ~10 km radius from Lake Lin. The white star represents the location of Lake Lin and the colored boundaries on the map represent known fires around Lake Lin. The numbers in the boundaries show the year of burns (top) and total area burned (bottom).

Figure 5: Reconstructed temperatures using three different indices over the last millennium. The three lines correspond to three different temperature indices after De Jonge et al. (2014).

Figure 6: Fire reconstructions from charcoal records from Alaskan lakes. a) The location of charcoal records in Alaska. All tundra ecoregions are highlighted in color based on Nowacki et al. (2001). The number in parentheses indicates the number of detected fires over the last millennium. A record that has a fire peak that does not pass the screen test is marked by an asterisk.

Figure 7: Map showing distances between Tungak Lake and known fire events. Orange patches represent the AD 2015 burn, and yellow patches represent fires prior to AD 2015. Light blue shades symbolize big lakes in the region. The values next to selected burns and Lake Lin represent burn year (top), total area burned (middle), and the distance from Tungak Lake (bottom in the parentheses).

Figure 8: Comparison between brGDGTs temperature reconstruction of the YK Delta and other previous records. Panel a) represents reconstructed temperatures of the YK Delta, Alaska over the last millennium. Panel b) represents arctic temperature synthesis from Alaska, Canada, Greenland, Europe and Russia (Kaufman et al., 2009). Panel c) represents average Alaskan temperature of four different locations excerpted from Kaufman et al. (2009) (black line). These Alaskan temperature reconstructions were based on varve thickness, tree rings and sediment (gray lines).

Rationale for age assumption of core top

Although wind can cause perturb the sediment-water interface in lakes and thus cause sediment mixing, wind-induced sediment resuspension at the lake bottom of Lake Lin is unlikely. According to Scheffer (1998), particles at the sediment-water interface will resuspend if wind-induced waves reach the bottom of the lake (when the wavelength of wind-induced waves exceeds twice the water depth). The wavelength is a function of fetch (the distance over which the waves have built up) and wind velocity. More detail of this equation can be found in Scheffer (1998). We found that the wavelength caused by NCEP/NCAR Reanalysis mean surface wind velocity at Lake Lin, which has a fetch of 33 m, is 0.004 m. This wavelength is less than twice the water depth (~1 m), and thus, wind induced mixing at the surface-water interface is unlikely. In fact, it is very unlikely for wind-induced waves to cause sediment mixing at Lin no matter how strong wind speed is because the fetch value at Lin is too small (Scheffer, 1998; Figure 2.7). Therefore, our assumption of the preservation of the core top is robust.

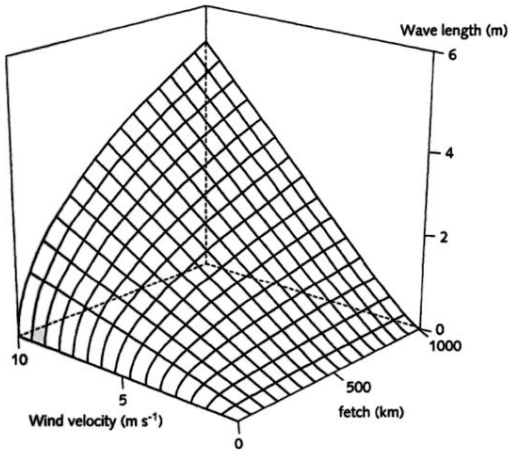

Fig. 2.7 Increase of wavelength (L_w) with fetch (F) and wind velocity (W) in deep water as described by Eq. 15.

(Scheffer, 1998)

Reference

Scheffer M (1998) *Ecology of Shallow Lakes*. Dordrecht: Kluwer Academic Publishers.

Supplementary figures

Figure A: Satellite image of Lake Lin (coring location denoted by orange marker; courtesy: ESRI).

Figure B: Landscape characteristics and vegetation near the study site (within 5 km radius of Lake Lin). a) Local landscape of the study site. b) Vegetation in the AD 2015 burn scar. Dominant vegetation types are grasses and herbs. c) Vegetation in the AD 1972 "old" burn scar. Grasses and mosses are the most common vegetation types. d) Vegetation in the unburned area. Lichen is the dominant vegetation type. (Photo credit: Stash Wislocki and Homero Pena)

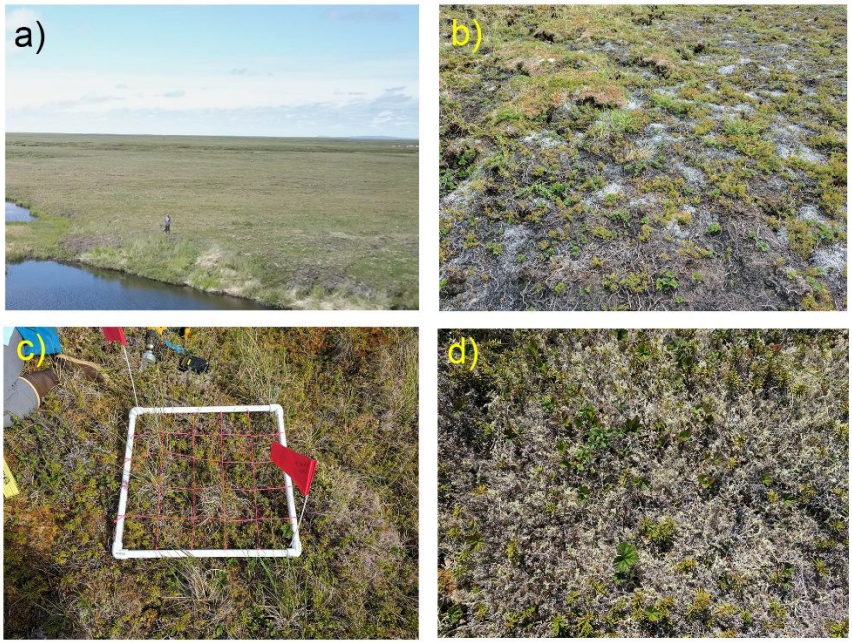

Figure C: NCEP/NCAR Reanalysis composite mean of surface wind in Alaska (AD 1948-2017; unit = m/s ; Kalney et al., 1996).

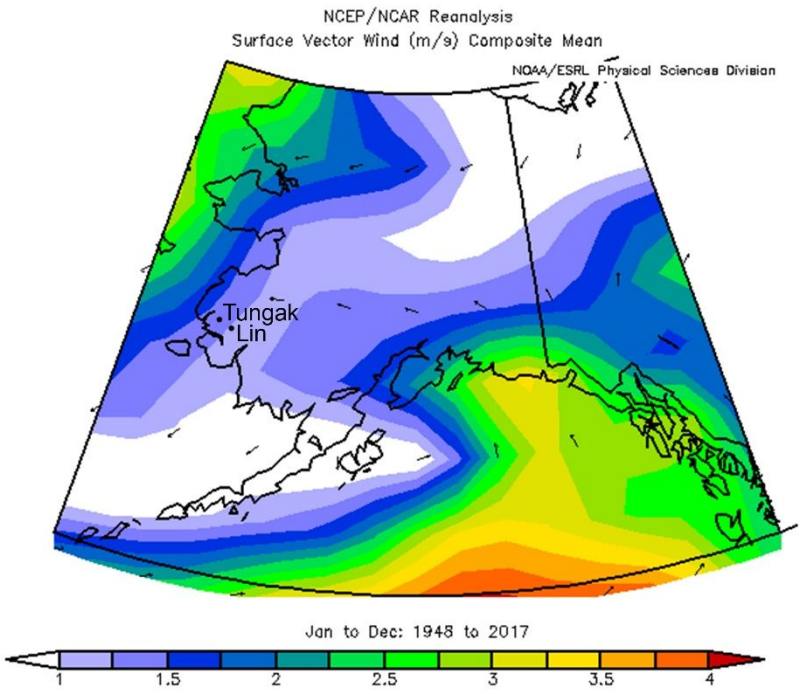

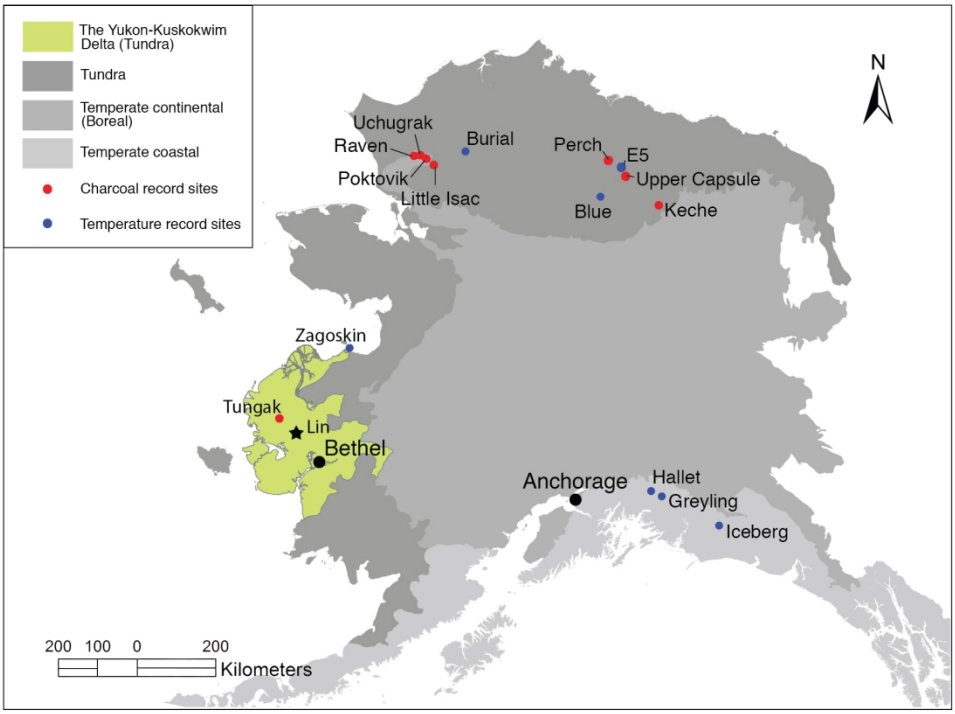

Figure 1. GIS maps of the study region, and locations of published Alaskan records. Map of Alaska with ecoregions represented in different colors (Nowacki et al., 2001). Green, dark gray, medium gray and light gray patches show the YK Delta, tundra, temperate continental and temperate coastal, respectively. The black circles denote major Alaskan cities. The black star represents Lake Lin, our study site. The red circles show locations of published charcoal records (Chipman et al., 2015; Higuera et al., 2011). The blue circles show locations of Alaskan temperature reconstructions (published: Kaufman et al., 2009; Bird et al., 2008; Mckay and Kaufman, 2008; Loso et al., 2006; Kurek et al., 2008; unpublished: Husain, 2017).

169x122mm (300 x 300 DPI)

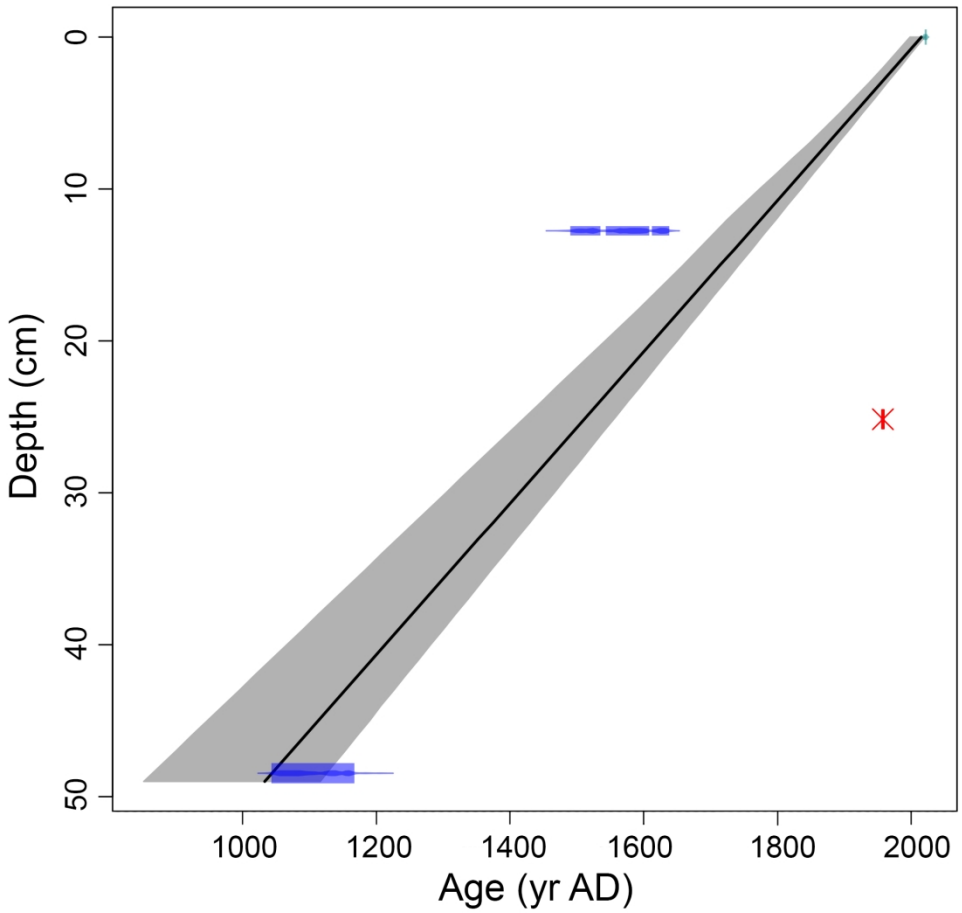

Figure 2: Age-depth model for Lake Lin with AMS 14C dates (blue). The black line shows the mean age-depth plot and the gray shading represents uncertainty of the age-depth plot at 95% confidence ranges. The light blue mark at the top right corner represents the coring year (AD 2017). The dark blue marks are radiocarbon dates. The red mark represents the excluded abnormally young radiocarbon date. The abnormally old radiocarbon date is not shown.

186x178mm (300 x 300 DPI)

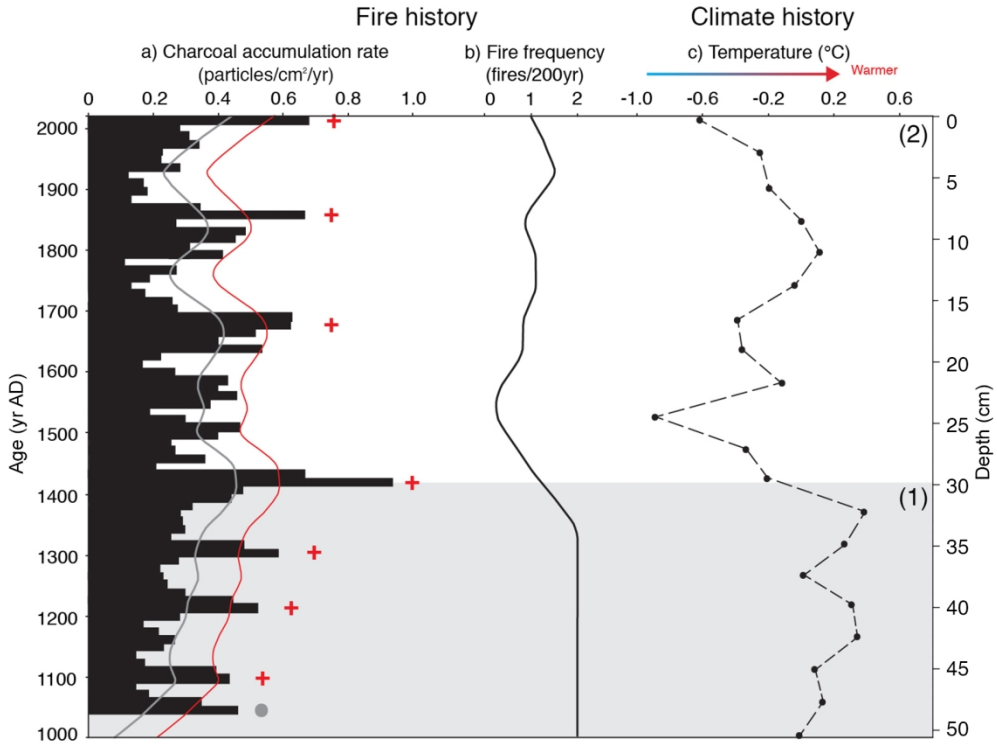

Figure 3: Fire and climate history of the YK Delta, Alaska. a) CHAR variability over the last millennium. Black bars represent CHAR throughout the core. The gray line represents CHAR background, while the red line shows the 90% threshold or cutoff. Peaks that passed the red line were counted as fire episodes as indicated by red plus symbol. A gray dot represents a major fire episode that failed CharAnalysis test. b) Fire frequency (number of fires over 200 years). c) The Reconstructed temperature of the region, based on MBT'5ME index. This composited plot was divided into two zones based on FRIs. Zone 1 (gray shading) represents the time from AD 1000-1420, and Zone 2 (white shading) represents the time between AD 1420 to present.

154x122mm (300 x 300 DPI)

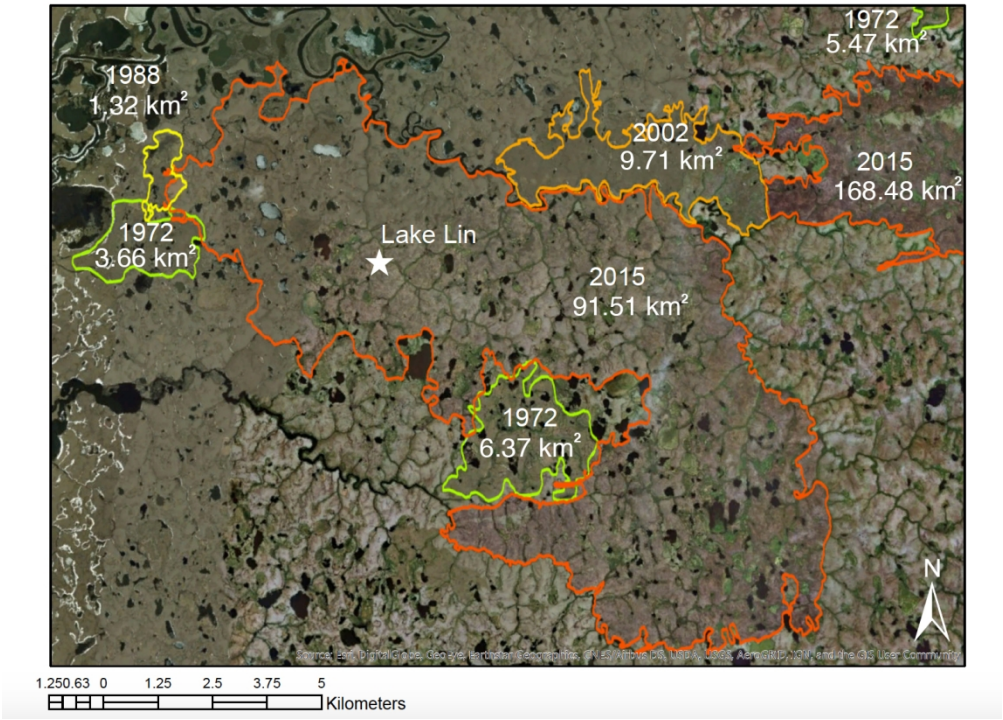

Figure 4: Map of Lake Lin and known wildfires within ~10 km radius from Lake Lin. The white star represents the location of Lake Lin and the colored boundaries on the map represent known fires around Lake Lin. The numbers in the boundaries show the year of burns (top) and total area burned (bottom).

279x208mm (144 x 144 DPI)

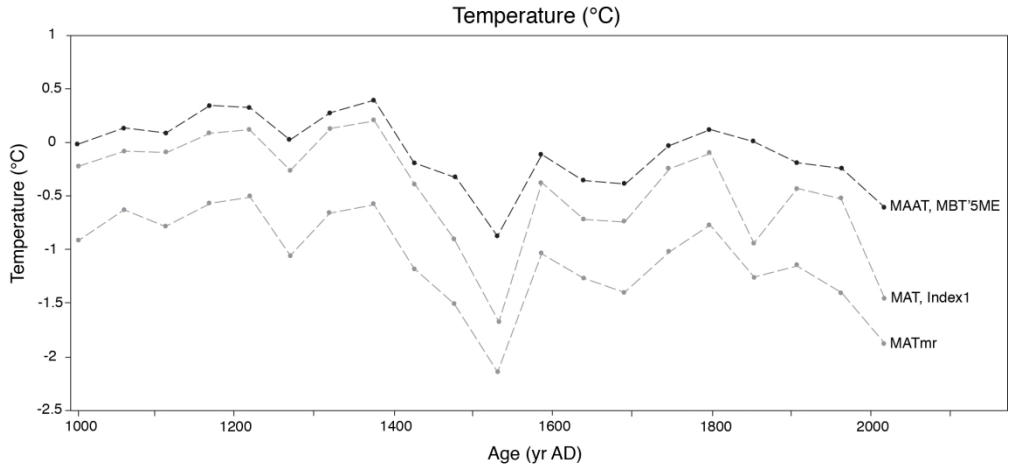

Figure 5: Reconstructed temperatures using three different indices over the last millennium. The three lines correspond to three different temperature indices after De Jonge et al. (2014).

192x91mm (300 x 300 DPI)

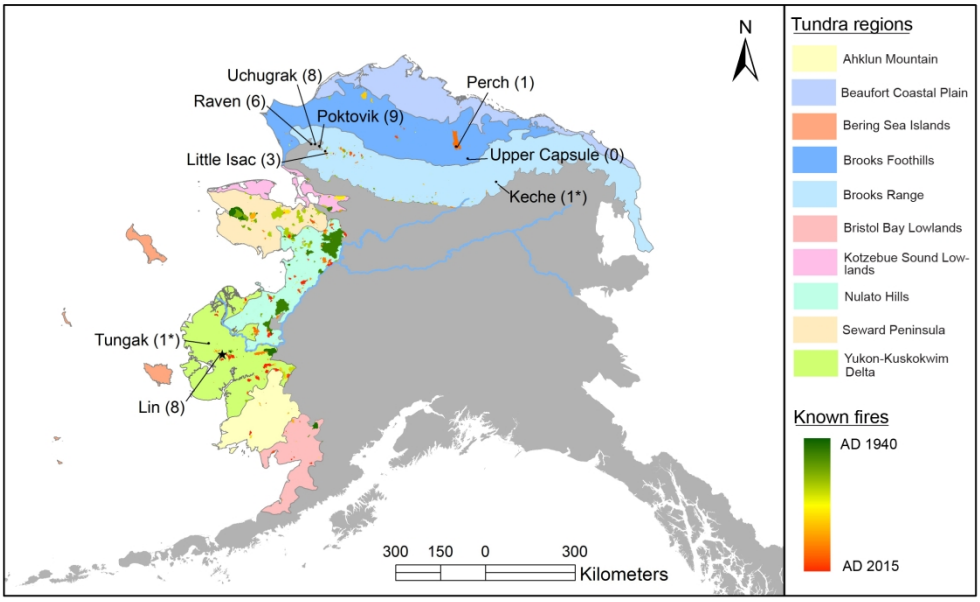

Figure 6: Fire reconstructions from charcoal records from Alaskan lakes. a) The location of charcoal records in Alaska. All tundra ecoregions are highlighted in color based on Nowacki et al. (2001). The number in parentheses indicates the number of detected fires over the last millennium. A record that has a fire peak that does not pass the screen test is marked by an asterisk.

193x120mm (300 x 300 DPI)

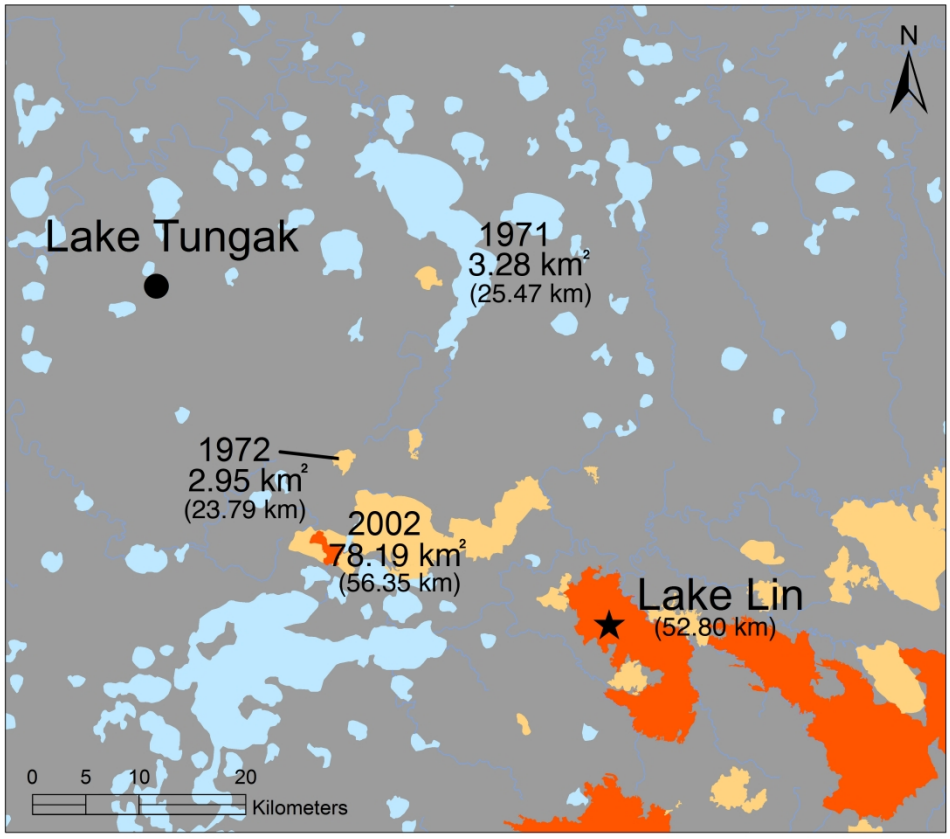

Figure 7: Map showing distances between Tungak Lake and known fire events. Orange patches represent the AD 2015 burn, and yellow patches represent fires prior to AD 2015. Light blue shades symbolize big lakes in the region. The values next to selected burns and Lake Lin represent burn year (top), total area burned (middle), and the distance from Tungak Lake (bottom in the parentheses).

381x327mm (300 x 300 DPI)

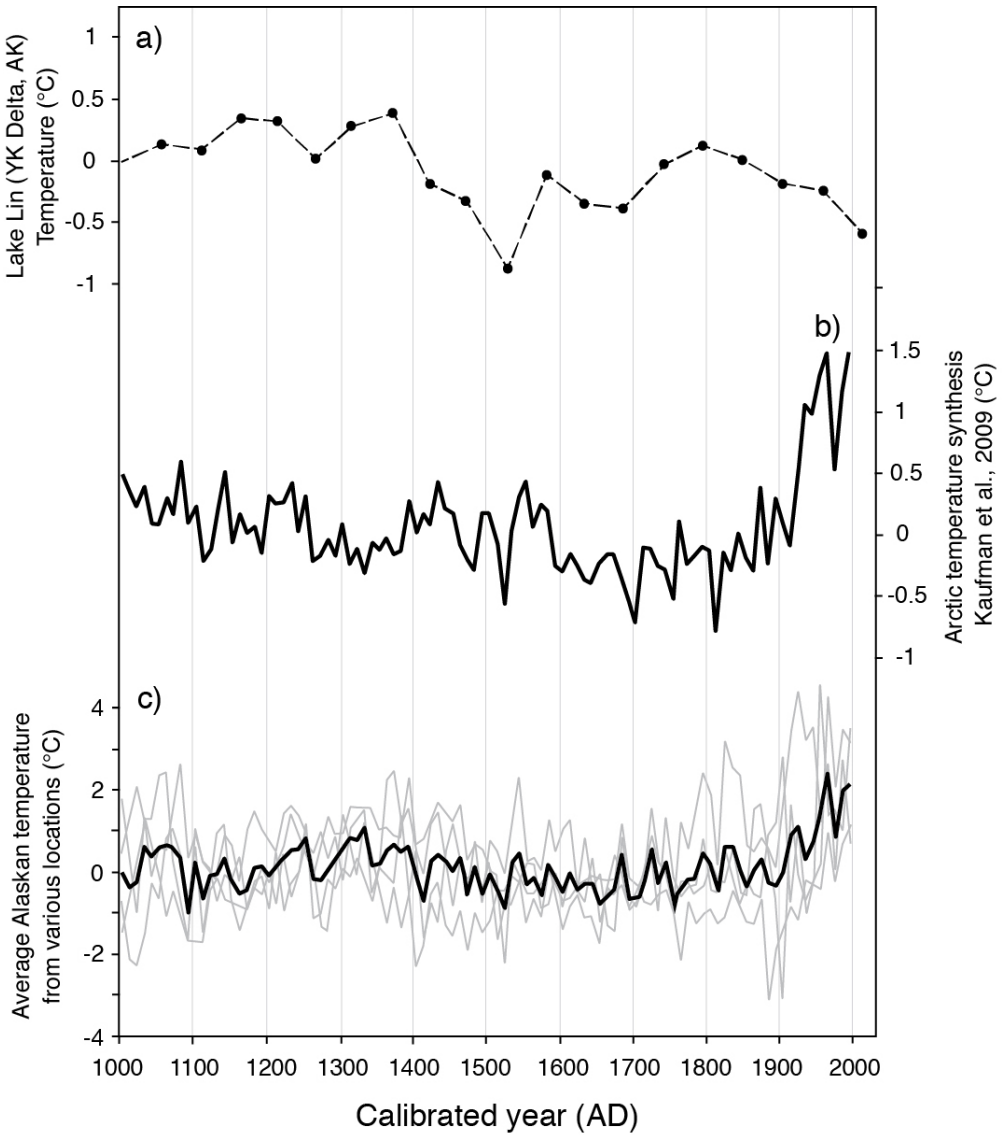

Figure 8: Comparison between brGDGTs temperature reconstruction of the YK Delta and other previous records. Panel a) represents reconstructed temperatures of the YK Delta, Alaska over the last millennium. Panel b) represents arctic temperature synthesis from Alaska, Canada, Greenland, Europe and Russia (Kaufman et al., 2009). Panel c) represents average Alaskan temperature of four different locations excerpted from Kaufman et al. (2009) (black line). These Alaskan temperature reconstructions were based on varve thickness, tree rings and sediment (gray lines).

90x102mm (300 x 300 DPI)